Society For Biomaterials

Novel hydrophilic nanostructured microtexture on direct metal laser sintered Ti–6Al–4V surfaces enhances osteoblast response *in vitro* and osseointegration in a rabbit model

AQ6 Sharon L. Hyzy,[1*] Alice Cheng,[2,3*] David J. Cohen,[1] Gustavo Yatzkaier,[4] Alexander J. Whitehead,[1] Ryan M. Clohessy,[1] Rolando A. Gittens,[5] Barbara D. Boyan,[1,2] Zvi Schwartz[1,6]

[1]Department of Biomedical Engineering, Virginia Commonwealth University, Richmond, Virginia
[2]Department of Biomedical Engineering, Georgia Institute of Technology, Atlanta, Georgia
[3]Department of Biomedical Engineering, Peking University, Beijing, China
[4]Private Oral Surgery Clinic, Ashkelon, Israel
[5]Center for Biodiversity and Drug Discovery, Institute for Advanced Scientific Research and High Technology Services (INDICASAT AIP), Panama City, Panama
[6]University of Texas Health Science Center at San Antonio, San Antonio, Texas

Received 3 October 2015; revised 21 March 2016; accepted 31 March 2016
Published online 00 Month 2016 in Wiley Online Library (wileyonlinelibrary.com). DOI: 10.1002/jbm.a.35739

Abstract: The purpose of this study was to compare the biological effects *in vivo* of hierarchical surface roughness on laser sintered titanium–aluminum–vanadium (Ti–6Al–4V) implants to those of conventionally machined implants on osteoblast response *in vitro* and osseointegration. Laser sintered disks were fabricated to have micro-/nano-roughness and wettability. Control disks were computer numerical control (CNC) milled and then polished to be smooth (CNC-M). Laser sintered disks were polished smooth (LST-M), grit blasted (LST-B), or blasted and acid etched (LST-BE). LST-BE implants or implants manufactured by CNC milling and grit blasted (CNC-B) were implanted in the femurs of male New Zealand white rabbits. Most osteoblast differentiation markers and local factors were enhanced on rough LST-B and LST-BE surfaces in comparison to smooth CNC-M or LST-M surfaces for MG63 and normal human osteoblast cells. To determine if LST-BE implants were osteogenic *in vivo*, we compared them to implant surfaces used clinically. LST-BE implants had a unique surface with combined micro-/nano-roughness and higher wettability than conventional CNC-B implants. Histomorphometric analysis demonstrated a significant improvement in cortical bone-implant contact of LST-BE implants compared to CNC-B implants after 3 and 6 weeks. However, mechanical testing revealed no differences between implant pullout forces at those time points. LST surfaces enhanced osteoblast differentiation and production of local factors *in vitro* and improved the osseointegration process *in vivo*. © 2016 Wiley Periodicals, Inc. J Biomed Mater Res Part A: 00A:000–000, 2016.

Key Words: additive manufacturing, animal model, dental implants, DMLS, laser sintering technology, titanium alloy

How to cite this article: Hyzy SL, Cheng A, Cohen DJ, Yatzkaier G, Whitehead AJ, Clohessy RM, Gittens RA, Boyan BD, Schwartz Z. 2016. Novel hydrophilic nanostructured microtexture on direct metal laser sintered Ti–6Al–4V surfaces enhances osteoblast response *in vitro* and osseointegration in a rabbit model. J Biomed Mater Res Part A 2016:00A:000–000.

INTRODUCTION

Osseointegration of implants into the jaw, hip, spine, or other bone is the ultimate clinical goal for endosseous implants. Titanium (Ti) is commonly used in bone-interfacing implants because of its desirable mechanical properties and ability to create a direct apposition with bone.[1,2] Ti alloys such as titanium–aluminum–vanadium (Ti–6Al–4V) are also popular and have shown success clinically.[3] The five-year success rate of dental implants has increased from 93.5% to 97.1% within the past decade, with higher survival and lower complication rates.[4] However, in dentistry and other orthopedic fields, patient and clinical variability affect implant outcomes. High variability in implant survival exists for hip replacements, with an

*These authors are Co-first Authors.
Conflict of Interest: One or more of the authors has received or will receive remuneration or other perquisites for personal or professional use AQ2 from a commercial or industrial agent in direct or indirect relationship to their authorship.
Correspondence to: Barbara D. Boyan, School of Engineering, Virginia Commonwealth University, 601 West Main Street, P.O. Box 843068, Richmond, Virginia 23284-3068. e-mail: bboyan@vcu.edu
Contract grant sponsor: AB Dental and a National Science Foundation Graduate Research Fellowship (to A.C.)
AQ1 Contract grant sponsor: SNI program from SENACYT, Panama (R.A.G.)
Contract grant sponsor: National Institute of Arthritis and Musculoskeletal and Skin Diseases (NIAMS) (USPHS Award Nos. AR052102 and AR068703)

estimated 5–20% revision rate for patients with total hip arthroplasty.[5] Osseointegration rates are significantly lower in compromised patients including smokers, diabetics, or those with low bone density.[6–8] In addition, an increasing number of cases require the use of custom or very specific implants. Although implants are made in a variety of shapes and sizes, the production costs and waste associated with manufacturing a single custom implant can decrease patient desire for implant therapy. Thus, a more cost-effective method of producing orthopedic and dental implants is necessary for a broad range of clinical cases and patient populations.

Much progress has been made in orthopedic and dental implant design within the past 20 years. During this time, our lab has focused on developing and characterizing new implant surfaces and understanding the physical parameters of these surfaces on biological response. Recently, the clinical implant research community has gained an interest in additive manufacturing, touting it as a "game changer" in the field.[9] Direct metal laser sintering (DMLS) is an additive manufacturing technique that can be used to build custom orthopedic and dental implants from Ti–6Al–4V powder.[10] Not only does this method save time, material, and money, but it also allows customized implants with micron-scale resolution.[11] Customized implants eliminate the need for further manipulation of the implanted material during surgery or piecing together multiple parts of material. Such advancements in manufacturing technology have shown positive results both *in vitro* and *in vivo* ~~animal models~~, and recently, these manufacturing methods have been implemented clinically.[10,12–14]

From a scientific perspective, manipulating chemical and physical parameters can alter the biological response at the surface. For decades, scientists have tried to understand what factors are needed to optimize the surface for increased cell attachment, osteoblast differentiation, and ultimately osseointegration with the surrounding and new bone. Our lab has shown the importance of wettability, surface micro- and nanoroughness, and implant macrostructure in increasing osteoblast response to implant surfaces.[15–18] These factors influence protein adsorption and cell response at the implant surface but have also been shown to affect osteoblastic differentiation and formation of an osteogenic environment at sites distal to the implant.[18,19] In addition, various animal models used by ours and other ~~labs~~ continue to explore osseointegration of new surfaces *in vivo* to translate between mechanistic studies and clinical relevance.[13,20,21]

Although small rodents are commonly used for preclinical studies due to their low price and availability, implants or surfaces must be designed with smaller dimensions to conform to these models.[20] Rabbits are a larger animal model that can be used with clinically relevant implant sizes, with various studies validating implant placement in rabbit tibias or femurs.[22–24] Rabbits comprise 35% of all animal studies and are the most used model in musculoskeletal research.[25]

In this study, we compared the biological response to Ti–6Al–4V surfaces and implants manufactured by either traditional milling using computer numerical control (CNC) technology or DMLS. We first compared osteoblast response to disks fabricated by CNC milling and then polished to yield a smooth surface (CNC-M) with disks fabricated by the laser-sintering technology (LST) followed by processing to generate smooth (LST-M), grit blasted (LST-B), and grit-blasted/acid etched (LST-BE) surfaces. To determine if LST-BE implants were osteogenic *in vivo*, we compared their osseointegration with commercially available CNC-B implants in a rabbit model. We hypothesized that laser sintered surfaces would induce osteoblast differentiation in a roughness-dependent manner and that laser sintered implants with post-fabrication surface roughness would osseointegrate in a manner comparable to, if not better than, clinically used CNC-manufactured and grit blasted implants.

MATERIALS AND METHODS

Surface manufacturing

All disks used for *in vitro* studies were 15 mm in diameter and 1 mm in height in order to fit snugly into wells in a 24-well plate. Grade 4 Ti–6Al–4V rods were cut using CNC milling and polished using aluminum oxide sandpaper (P240, Norton Abrasive, Paris, France) to yield a smooth surface (CNC-M). LST surfaces were sintered as disks as published previously.[12] Briefly, Ti–6Al–4V particles 24–45 μm in diameter were sintered with a Ytterbium fiber laser (EOS, EmbH Munchen, Germany) using a scanning speed of 7 m s^{-1}, wavelength of 1054 nm, continuous power of 200 W, and laser size of 0.1 mm. LST-M surfaces were polished as above to produce a smooth surface. LST-B surfaces were blasted with calcium phosphate particles in a proprietary method (AB Dental, Ashdod, Israel). LST-BE surfaces were laser sintered, blasted with calcium phosphate particles and then acid etched for 90 min in 10% of a 1:1 ratio of maleic and oxalic acids (Sigma-Aldrich, St. Louis, Missouri) in distilled water. All disks and implants were generously provided as a gift from AB Dental.

Scanning electron microscopy

Scanning electron microscopy (SEM, Hitachi SU-70, Tokyo, Japan) was used to obtain low and high magnification images of surfaces and implants. Images were taken at an accelerating voltage of 4 kV, objective aperture of 30 μm, and a working distance of 4 mm. Various magnifications were used to image locations across samples and the most representative images chosen for each sample. High magnification images were used to qualitatively assess surface nano-roughness.

X-ray photoelectron spectroscopy

The surface chemical composition was determined by X-ray photoelectron spectroscopy (XPS, ThermoFisher ESCAlab 250, Waltham, Massachusetts). Survey scans were taken using an Al-Kα X-ray source and a spot size of 500 μm. Six locations were surveyed for each implant, with two implants

per group analyzed for a total average across $n = 12$ locations.

~~X-ray dispersive~~ spectroscopy

Chemical analysis was performed by energy dispersive X-ray spectroscopy (EDX, Hitachi SU-70, Tokyo, Japan) at an accelerating voltage of 15 kV and a working distance of 15 mm. Scans were performed for 50 s, and atomic percentages were recorded as the average of six scans per group.

Laser confocal microscopy

Laser confocal microscopy (LCM, LEXT OLS4000, Olympus, Center Valley, Pennsylvania) was used to assess average surface micro-roughness (S_a) and peak-to-valley height (S_z). Scans were taken over a 644 μm^2 area with a 20× objective and 0.5 μm step size. A cutoff wavelength of 100 μm was used to exclude effects of waviness. Three measurements were taken per sample, with two samples per group analyzed ($n = 6$).

Contact angle and immersion analysis

Wettability of surfaces was assessed through sessile drop contact angle. A 4 μL drop of distilled water was deposited on surfaces using a goniometer (Rame-hart model 200, Succasunna, New Jersey) and was analyzed with DROPimage (Rame-hart). For hydrophilic samples, surfaces were dried for 1 min with flowing nitrogen between measurements. Five drops were analyzed per sample, with two samples per group ($n = 10$). Reported measurements are the mean and standard deviation of the left and right contact angles for each group. Images of implant immersion into distilled water were captured to evaluate implant wettability qualitatively.[26]

Cell culture

A cell culture model established by our lab for analyzing osteoblast response to clinically relevant surfaces was used to assess cell response to laser sintered surfaces.[27,28] MG63 osteoblast-like cells (ATCC, Manassas, Virginia) or normal human osteoblasts (NHOst, Lonza, Walkersville, Maryland) were plated onto tissue culture polystyrene (TCPS), CNC-M, LST-M, LST-B, and LST-BE surfaces at a density of 10,000 cells/cm^2. MG63 cells were used before passage 15 while NHOsts were between passage 4 and 7. Cells were cultured in Dulbecco's modified Eagle's medium supplemented with 10% fetal bovine serum (Life Technologies, Carlsbad, California), 50 U/mL penicillin, and 50 μg/mL streptomycin in a 24-well plate. Cells were fed 24 h after plating and every 48 h thereafter until cells reached confluence on TCPS (approximately 5 days after plating for MG63 cells and 7 days for NHOsts). The medium was replaced at confluence. All statistical analyses for *in vitro* studies were conducted using one-way analysis of variance (ANOVA) with Bonferroni-post-correction and a p ~~value~~s of <0.05 indicating significance.

Secreted factors analysis

At 24 h post-confluence, conditioned media were collected, cell monolayers were rinsed twice with PBS and lysed in 0.05% Triton X-100, and both were frozen overnight before analysis. Cell lysates were homogenized by sonication. DNA content (QuantiFluor, Promega, Madison, Wisconsin) and alkaline phosphatase specific activity (p-nitrophenol release from p-nitrophenyl phosphate at pH 10.25, normalized to the protein content of lysate) were measured.

Culture supernatants were used to quantify protein release by cells. Enzyme-linked immunosorbent assays were used to quantify osteocalcin (Alfa Aesar, Ward Hill, Massachusetts), osteoprotegerin (OPG, R&D Systems, Minneapolis, Minnesota), vascular endothelial growth factor A (VEGF, R&D Systems), fibroblast growth factor 2 (FGF2, R&D Systems) and bone morphogenetic protein 2 (BMP2, PeproTech, Rocky Hill, New Jersey) following manufacturer's instructions. Immunoassay results for each culture were normalized to total cell number.

mRNA analysis

In a separate set of culture, cells for mRNA analysis were incubated with fresh media for 12 h after cells reached confluence on TCPS. TRIzol® was used to isolate RNA according to manufacturer's instructions and reverse transcribed into cDNA (High Capacity cDNA Kit, Life Technologies, Carlsbad, California). The cDNA was used for quantitative real-time polymerase chain reaction with SYBR Green (Life Technologies). Known dilutions of cDNA were used to generate standard curves and mRNA of integrin subunits α2 (F: ACTGTTCAAGGAGGAGAC; R: GGTCAAAGGCTTGTTTAGG) and β1 (F: ATTACTCAGATCCAACCAC; R: TCCTCCTCA TTTCATTCATC), and were normalized to the expression of glyceraldehyde 3-phosphate dehydrogenase (GAPDH, F: GCTCTCCAGAACATCATCC; R: TGCTTCACCACCTTC TTG).

Implant manufacturing

All implants were 3.7 mm in diameter and 8 mm in length and manufactured by AB Dental. Commercially available machined implants were fabricated using a traditional CNC manufacturing process and treated with a proprietary bioresorbable blasting method (AB Dental, Ashdod, Israel) to induce surface roughness (CNC-B). LST implants were laser sintered from Ti–6Al–4V powder as described above, blasted with calcium phosphate, and subsequently acid etched in the same manner used to generate LST-BE disk surfaces. All implants were sterilized with 2.5 Mrad of gamma radiation before use.

Surgical procedure

Skeletally mature, male New Zealand white rabbits weighing 4 ± 0.25 kg were obtained from Harlan Laboratories (Rossdorf, Germany). Each rabbit received two implants: a CNC-B implant placed in its left femur and an LST-BE implant placed in its right femur. Rabbits were given full anesthesia through flowing isoflurane. A 3 cm skin incision was made laterally at the distal femur, and muscle and soft tissue were separated. Drilling was carried out at low speed and

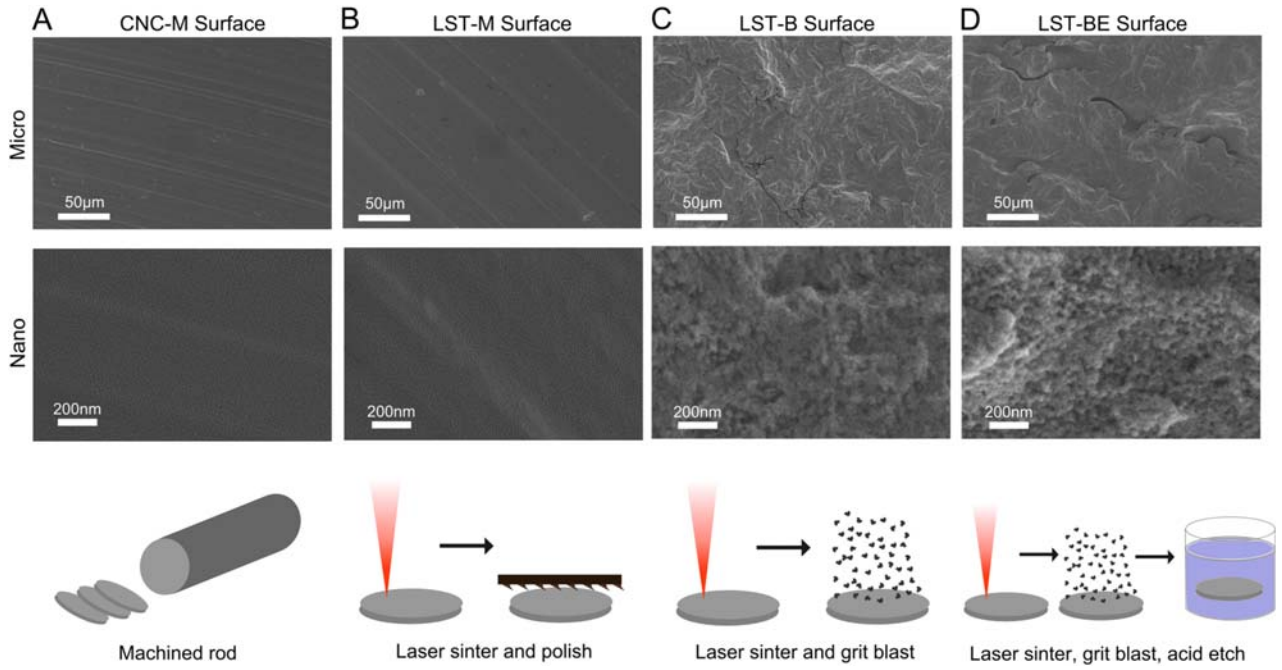

COLOR

FIGURE 1. SEM micrographs of CNC-M (A), LST-M (B), LST-B (C), and LST-BE (D) surfaces used for *in vitro* studies. A low magnification view shows micro-roughness (top) and high magnification view shows nano-roughness (middle). CNC-M surfaces were cut from a rod (A, bottom), while LST-M, LST-B, and LST-BE surfaces were produced by laser sintering with further surface treatment (B–D, bottom).

was accompanied by physiological saline irrigation. CNC-B implants were placed transaxially in the distal right femur, and LST-BE implants were implanted into the contralateral (left) femur. Each rabbit received one implant in each femur, with eight animals per time point and analysis. The cover screw remained above bone level, periosteum and muscle was reapproximated, and a simple running suture technique was used to close the surgical site skin incision. Animals were euthanized 3 or 6 weeks after implantation. Implants and surrounding bone were harvested for microcomputed tomography (microCT), histomorphometry, and mechanical testing (described below). The Animal Research Committee approved animal protocols at the University of Goethe (Frankfurt, Germany) and guidelines for the care and use of laboratory animals were observed. Statistical analysis of the histologic assessment of bone-implant contact (BIC) was conducted using one-way ANOVA and Tukey's tests with a p value~~s~~ of 0.05. Student's t test, with a p value~~s~~ of 0.05 indicating significance was used for comparison between two groups in the histologic ~~assessment~~, microCT, and mechanical testing.

Histology

Animals were euthanized at each time point, and femurs were harvested and ~~then were~~ fixed in 10% neutral buffered formalin. Eight implants were examined for each condition, and six implants measured for 3 week machined implants. Samples were embedded in methyl methacrylate. Histological sections longitudinal to the implant and transaxial to the animal were obtained from each sample (Histion LLC, Everett, Washington). Each section was stained using Stevenel's Blue.[29–31]

Slides were imaged using transmitted light bright field on a Zeiss Observer Z1 (Oberkochen, Germany) microscope equipped with a 10× objective and 10× optical zoom. Images were captured by an AxioCam MRc5 camera and were analyzed with Zeiss ZEN Pro Blue Edition software. The trabecular and cortical perimeter of each implant were measured using the curve (polygon) tool; the perimeter of the implant directly adjacent to the cortical bone was measured as cortical perimeter and the remainder as trabecular bone. BIC was assessed in three measurements: trabecular BIC, cortical BIC, and total BIC. Contact percentage was found by dividing the length of contact in the cortical and trabecular regions by the cortical and trabecular perimeters, respectively. The total BIC was calculated by summing both lengths of contact and dividing by the total perimeter of the implant.

MicroCT analysis

MicroCT (Bruker SkyScan 1173, Kontich, Belgium) was performed on rabbits 3 and 6 weeks after implantation. Eight implants were examined for each condition, and six implants measured for 3 week machined implants. Samples were scanned at a resolution of 1120 × 1120 pixels, using a 1.0 mm aluminum filter, a source voltage of 130 kV, source current of 61 μA, image pixel size of 18.69 μm, exposure of 350 ms, rotation step of 0.1°, and averaging and random movement correction every 10 frames. A standard Feldkamp reconstruction was performed on a subset of samples using NRecon software (Bruker, Kontich, Belgium) with a Gaussian smoothing kernel of zero and a beam hardening correction of 12%. BIC was determined by analyzing reconstructed scans in CTAn image analysis software

TABLE I. Average Roughness and Peak-to-Valley Heights of CNC-M, LST-M, LST-B, and LST-BE Surfaces

Sample	Average (S_a) (μm)	Peak-to-valley height (S_z) (μm)
CNC-M	1.42 ± 0.10	28.59 ± 3.61
LST-M	1.71 ± 0.05	35.26 ± 11.59
LST-B	2.39 ± 0.28	49.40 ± 8.61
LST-BE	2.94 ± 0.32	57.66 ± 7.33

(Bruker, Kontich, Belgium). Sagittal cross sections were thresholded to analyze implant volume within a 25 μm radius of the inner periphery. The image was then thresholded again to remove the implant by shrink wrapping the region of interest and despeckling the image. The bone volume within a 25 μm radius of the outer implant periphery was then analyzed by thresholding and despeckling the region of interest. The quotient of the bone volume and implant volume, multiplied by 100, was calculated as the total BIC.

Mechanical testing

Pull out testing was performed as a commonly used technique for evaluating mechanical properties of implant osseointegration in a rabbit femur model (MTS Insight 30; MTS Systems Corp., Eden Prairie, Minnesota).[32] In contrast to evaluating bone contact at the interface with torsional testing, pull out testing evaluates the quality of new bone formation around the implant.[33] A custom abutment fabricated by AB Dental was screwed completely into the implant and then was pulled at a crosshead speed of 5 mm/min according to ASTM standard 543-13. Axial pull-out strengths were recorded and the load was monitored for force at failure (N). Three animal-matched pairs of implants were examined 3 weeks after implantation and five pairs of implants were examined 6 weeks post-implantation.

RESULTS

Surface roughness and topography

All surfaces showed varying degrees of surface roughness. CNC-M and LST-M surfaces were smooth at both the micro- and nanoscale [Fig. 1(A,B)]. Both LST-B and LST-BE surfaces possessed similar micro-roughness and homogeneously distributed nanostructures [Fig. 1(C,D)]. LCM analysis showed increasing average surface roughness (S_a) for CNC-M (1.42 ± 0.10 μm), LST-M (1.71 ± 0.05 μm), LST-B (2.39 ± 0.28 μm), and LST-BE (2.94 ± 0.32 μm) (Table I). In the same manner, peak-to-valley height (S_z) increased for CNC-M (28.59 ± 3.61 μm), LST-M (35.26 ± 11.59 μm), LST-B (49.40 ± 8.61 μm), and LST-BE (57.66 ± 7.33 μm). Though blasting with calcium phosphate and acid etching both resulted in increased S_a and S_z compared to smooth surfaces, the increase of roughness on LST-B surfaces compared to LST-M was larger than the increase in roughness on LST-BE surfaces compared to LST-B surfaces.

TABLE II. EDX Elemental Analysis of CNC-M, LST-M, LST-B, and LST-BE Surfaces

Sample	Concentration [atomic % ± SD]			
	Ti	Al	V	O
CNC-M	86.6 ± 1.1	9.3 ± 1.2	4.0 ± 0.2	–
LST-M	87.1 ± 1.1	8.9 ± 1.4	4.0 ± 0.3	–
LST-B	59.1 ± 1.5	5.8 ± 0.5	2.5 ± 0.1	32.6 ± 1.6
LST-BE	87.8 ± 0.5	8.3 ± 0.7	3.9 ± 0.2	–

TABLE III. Sessile Drop Contact Angle of CNC-M, LST-M, LST-B, and LST-BE Surfaces

Sample	Contact angle (°) ± SD
CNC-M	108 ± 8
LST-M	111 ± 5
LST-B	<20
LST-BE	25 ± 7

Elemental analysis

Elemental composition analysis by EDX showed a prominence of Ti, followed by Al and V elements on all surfaces (Table II). Ti, Al, and V were present on CNC-M, LST-M, and LST-BE surfaces at similar levels. However, LST-B surfaces had reduced Ti, Al, and V and ~~a~~ more O compared to other surfaces.

Surface wettability

Contact angle measurements showed that LST-B had significantly lower contact angle and, therefore, higher surface wettability, compared to all other surfaces (Table III). The contact angles of CNC-M (108 ± 8°) and LST-M (111 ± 5°) were not significantly different from each other. However, micro-rough LST-B and LST-BE surfaces were hydrophilic with contact angles of <20° and 25 ± 7°, respectively.

In vitro cell response

DNA was higher in MG63 cells cultured on LST ~~surfaces~~ than on CNC-M [Fig. 2(A)]. Alkaline phosphatase specific activity [Fig. 2(B)], osteocalcin [Fig. 2(C)], osteoprotegerin [Fig. 2(D)], FGF2 [Fig. 2(F)], and BMP2 [Fig. 2(G)] were higher in MG63 cells on LST-B and LST-BE surfaces than cells on smooth (CNC-M and LST-M) surfaces. VEGF was only higher on LST-BE surfaces in comparison to M and LST-M surfaces [Fig. 2(E)]. mRNA levels of ITGA2 [Fig. 2(H)] and ITGB1 [Fig. 2(I)] increased on LST-B and LST-BE surfaces in comparison to CNC-M surfaces, but there was no difference in expression due to the acid etched surface.

While MG63 and NHOst responded similarly on the surfaces examined, the response varied for the specific factors measured. Osteocalcin secreted by NHOst was higher on all LST surfaces in comparison to CNC-M, and was higher on LST-B and LST-BE surfaces compared to LST-M surfaces [Fig. 3(A)]. OPG was increased on LST-B and LST-BE in comparison to CNC-M and LST-M surfaces [Fig. 3(B)]. VEGF was increased on LST-B and LST-BE surfaces in comparison to CNC-M and LST-M surfaces, and was significantly higher on

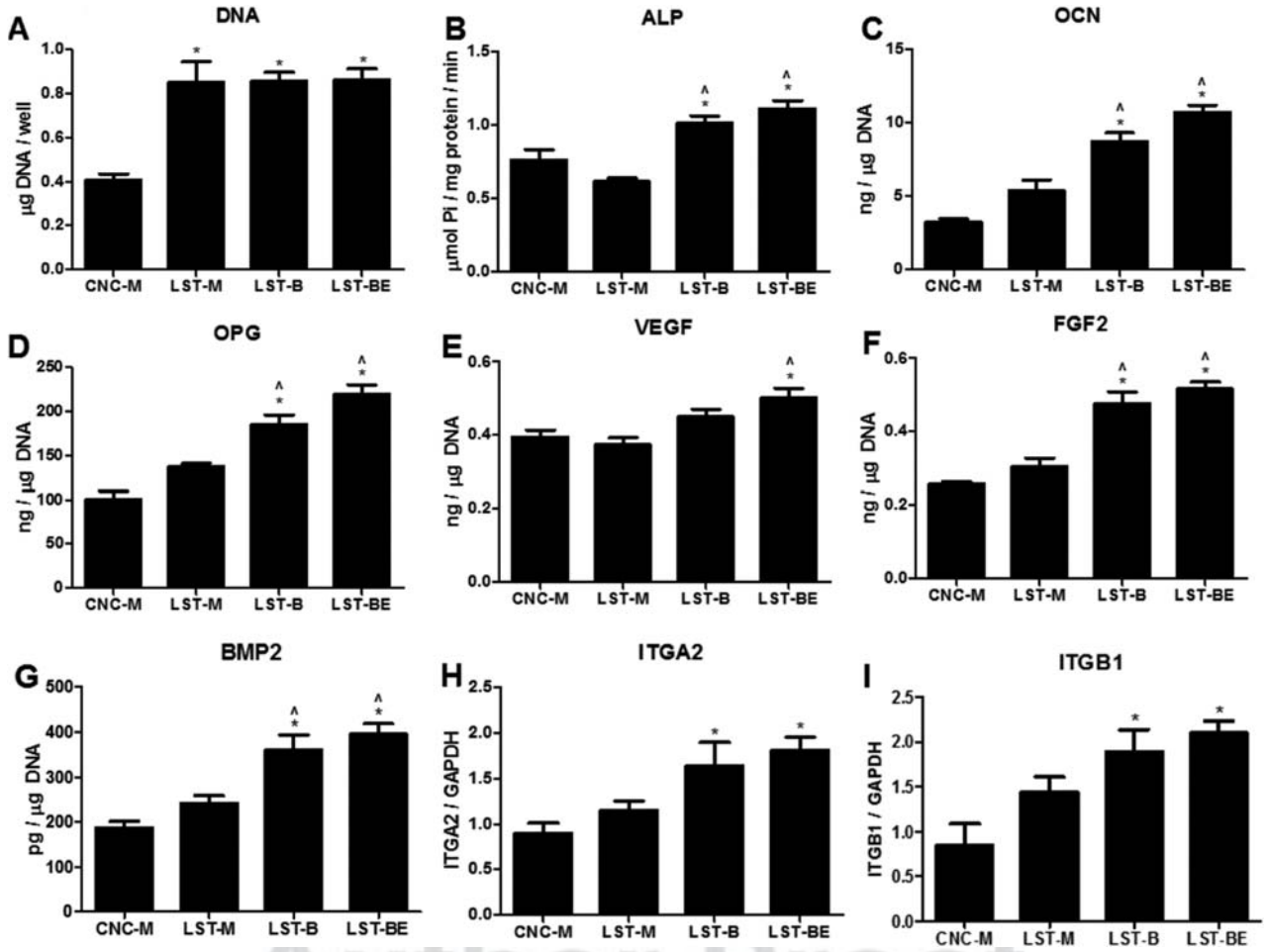

FIGURE 2. MG63 cell response to CNC-M, LST-M, LST-B, and LST-BE surfaces. DNA content (A) and alkaline phosphatase specific activity (B) were analyzed in cell lysates. Osteocalcin (C) vascular endothelial growth factor A (D), fibroblast growth factor 2 (E), and bone morphogenetic protein 2 (F) were measured in cell-conditioned media. mRNA levels of ITGA2 (G) and ITGB1 (H) were measured analyzed in cell media 24 h after confluence. $p < 0.05$, * versus CNC-M,^ versus LST-M, # versus LST-B.

LST-BE surfaces in comparison to LST-B surfaces [Fig. 3(C)]. BMP2 was higher on LST-B and LST-BE surfaces than on M and further increased on LST-BE surfaces in comparison to LST-B surfaces [Fig. 3(D)].

Implant surface roughness

CNC-B implants were manufactured by a traditional CNC manufacturing process, and LST-BE implants were manufactured via laser sintering. CNC-B and LST-BE implants underwent different surface treatments; however, both implants F4 possessed micro- and nano-roughness [Fig. 4(A,B)]. Although micro-roughness was similar for CNC-B and LST-BE implants, nano-roughness was quite different. LST-BE implants possessed distinct nanostructures on the surfaces while CNC-B implants did not have such distinct nanofeatures.

Implant surface chemistry

Surface chemistry analysis by XPS showed mainly Ti, O, and C on implant surfaces, with <3% of F, P, Al, and Si detected T4 on CNC-B implants only (Table IV).

Implant wettability

Sessile drop contact angle on the coronal, non-threaded portion of the implant showed a relatively more hydrophobic surface on CNC-B implants ($85 \pm 2°$) compared to LST-BE implants (<20°) [Fig. 4(C)]. Immersion of implants into distilled water showed a similar trend [Fig. 4(D)]. Water was drawn up the sides of the LST implant when immersing, indicating a hydrophilic surface. When pulling the implant out of water, more water was retained on the LST-BE implant compared to the CNC-B implant.

Histology

Histological analysis of CNC-B and LST-BE implants at 3 weeks [Fig. 5(A)] and 6 weeks [Fig. 5(B)], revealed differen- F5 ces in BIC values for each implant. BIC for LST implants was found to be significantly higher than in the machined implants at both the 3 week and 6 week time points [Fig. 5(C,D)]. Cortical BIC at 3 weeks was significantly lower than total or trabecular BIC for both CNC-B and LST-BE implants, although there were no differences in trabecular BIC at 3 weeks. Total BIC in the LST-BE group was statistically

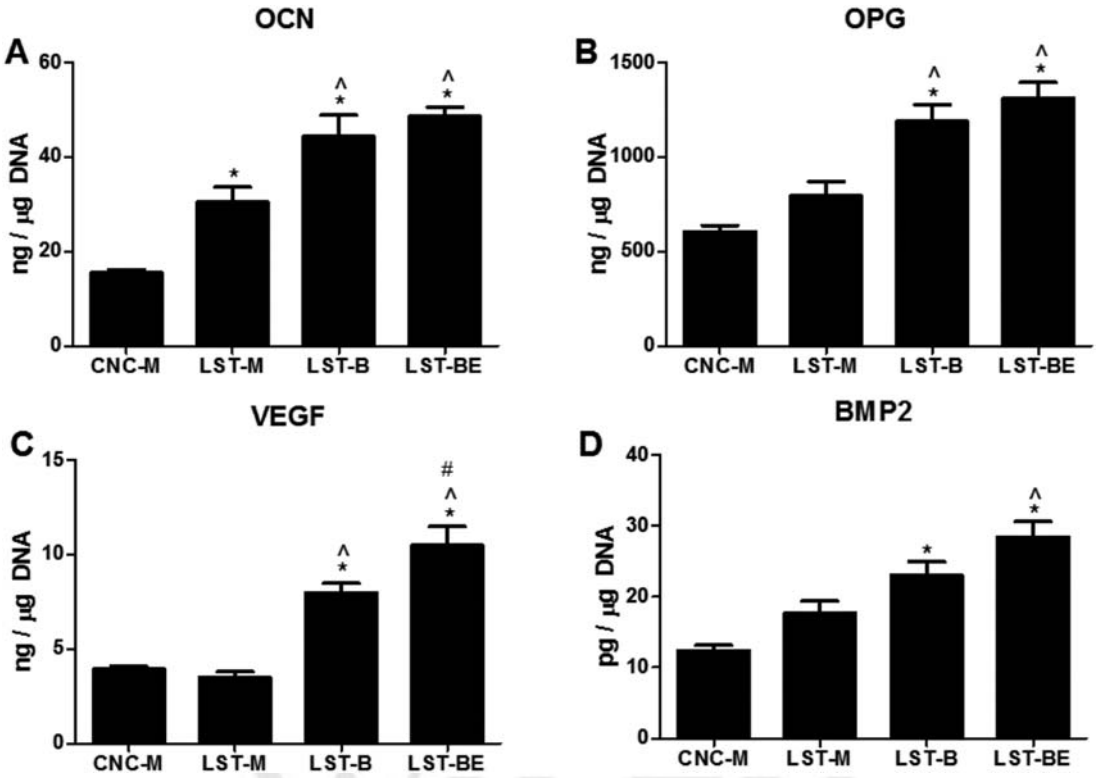

FIGURE 3. NHOst cell response to CNC-M, LST-M, LST-B, and LST-BE surfaces. Osteocalcin (A), osteoprotegerin (B), vascular endothelial growth factor (C), and bone morphogenetic proteins (D) were upregulated on LST-B and LST-BE surfaces. $p < 0.05$. * versus CNC-M, ^ versus LST-M, # versus LST-B.

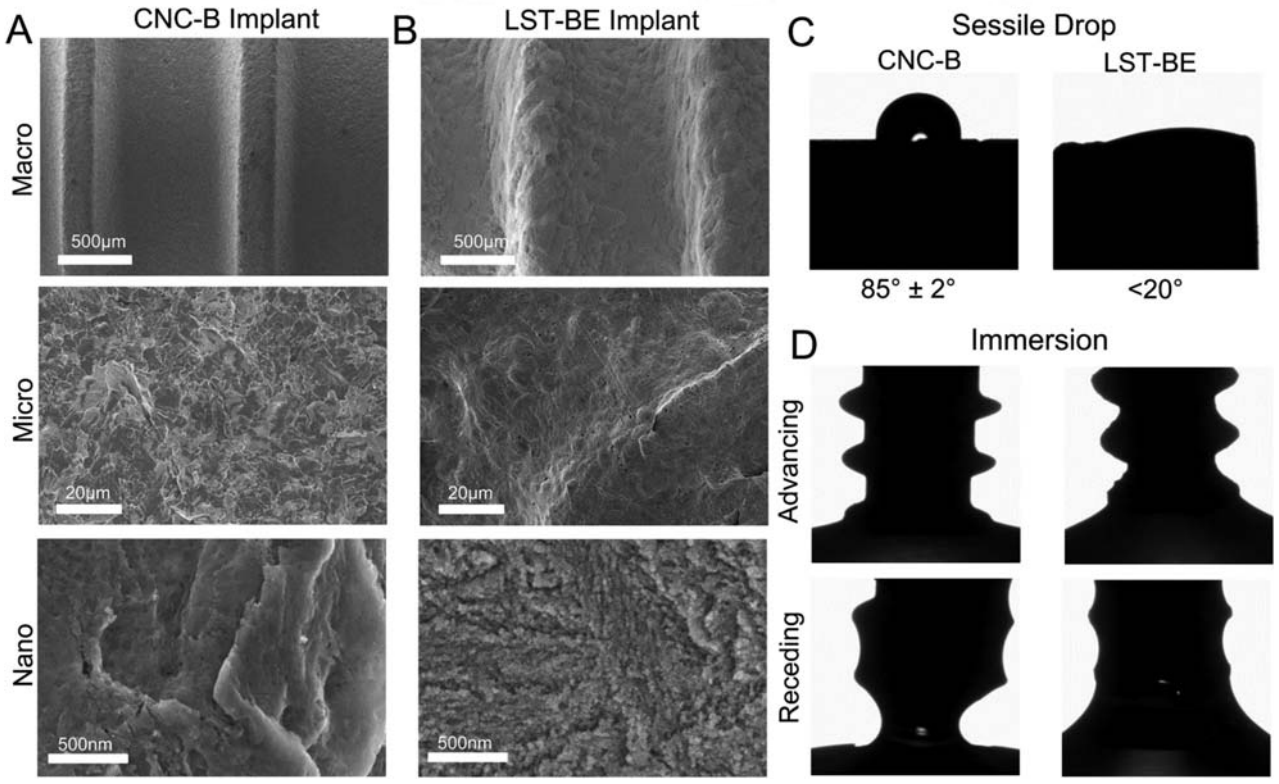

FIGURE 4. Scanning electron micrographs showing macro (top), micro (middle), and nano-roughness (bottom) of CNC-B (A) and LST-BE (B) implants. Sessile drop contact angles of CNC-M (left) and LST-BE (right) implants (C) and immersion analysis of wettability.

TABLE IV. XPS Elemental Analysis of CNC-B and LST-BE Implant Surfaces

	Concentration [atomic % ± SD]						
Sample	Ti	O	C	F	P	Al	Si
CNC-B	14.5 ± 1.2	51.1 ± 2.7	26.3 ± 4.3	2.2 ± 1.9	2.8 ± 1.4	1.7 ± 1.8	1.3 ± 1.4
LST-BE	9.4 ± 1.7	39.1 ± 1.7	39.5 ± 9.1	8.1 ± 4.2	–	–	–

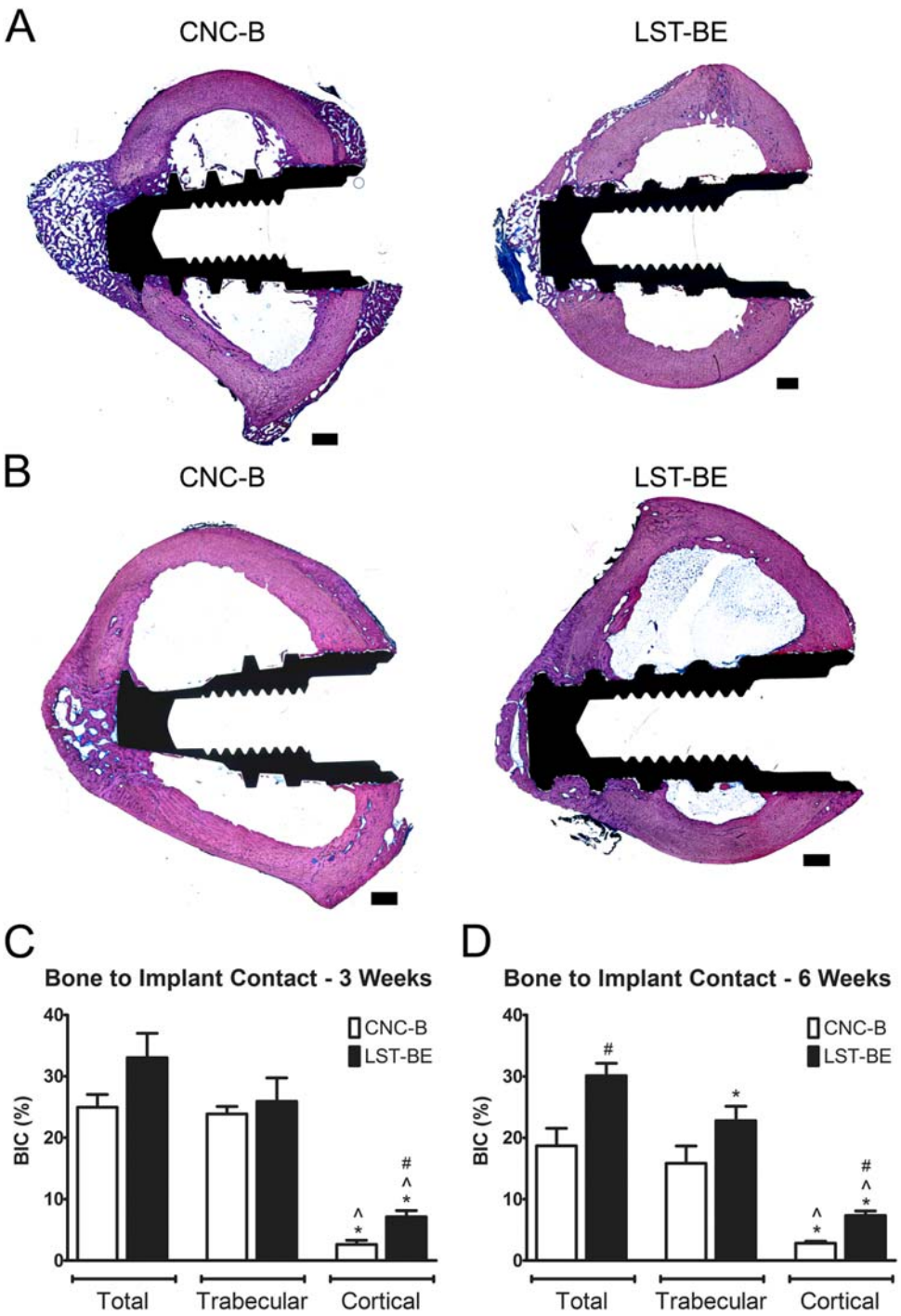

COLOR

FIGURE 5. Histology stained with Stevenel's Blue of CNC-B implants (left) and LST-BE implants (right) implanted in rabbits after 3 (A, $n = 6$–8) and 6 weeks (B, $n = 8$). BIC analyzed via histology images after 3 weeks (C) and 6 weeks (D) of implantation. Scale bars are 670 μm. One-way ANOVA with Bonferroni correction, $p < 0.05$, * versus total, ^ versus trabecular. Unpaired t test, $p < 0.05$, # versus CNC-B implant.

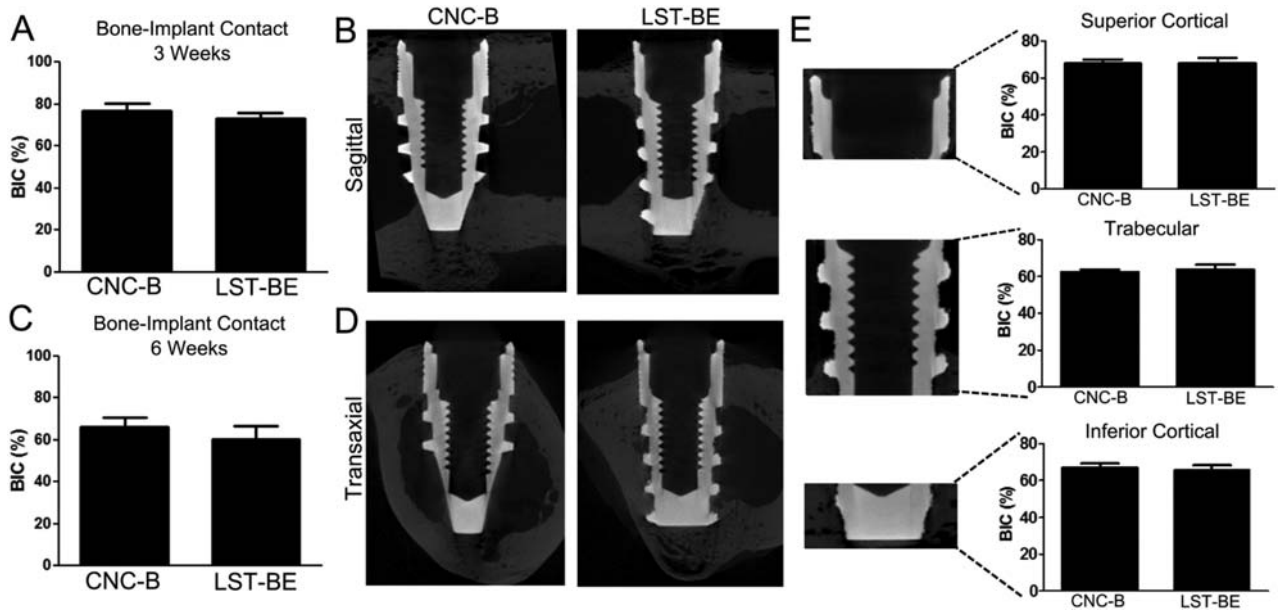

FIGURE 6. BIC values after 3 weeks (A, $n = 6$–8) and 6 weeks (C, $n = 8$) of implantation. MicroCT sagittal (B) and transaxial (D) cross sectional images of CNC-B (left) and LST-BE (right) implants after 6 weeks of implantation. Superior cortical (top), trabecular (middle), and inferior cortical (bottom) regions were analyzed for BIC as well (E).

higher than that in the machined group at 6 weeks. Trabecular BIC of LST-BE implants was significantly lower than total BIC at 6 weeks but was not significantly different from trabecular BIC of CNC-B implants. Cortical BIC values for both CNC-B and LST-BE implants were lower than total and trabecular BIC values at 6 weeks.

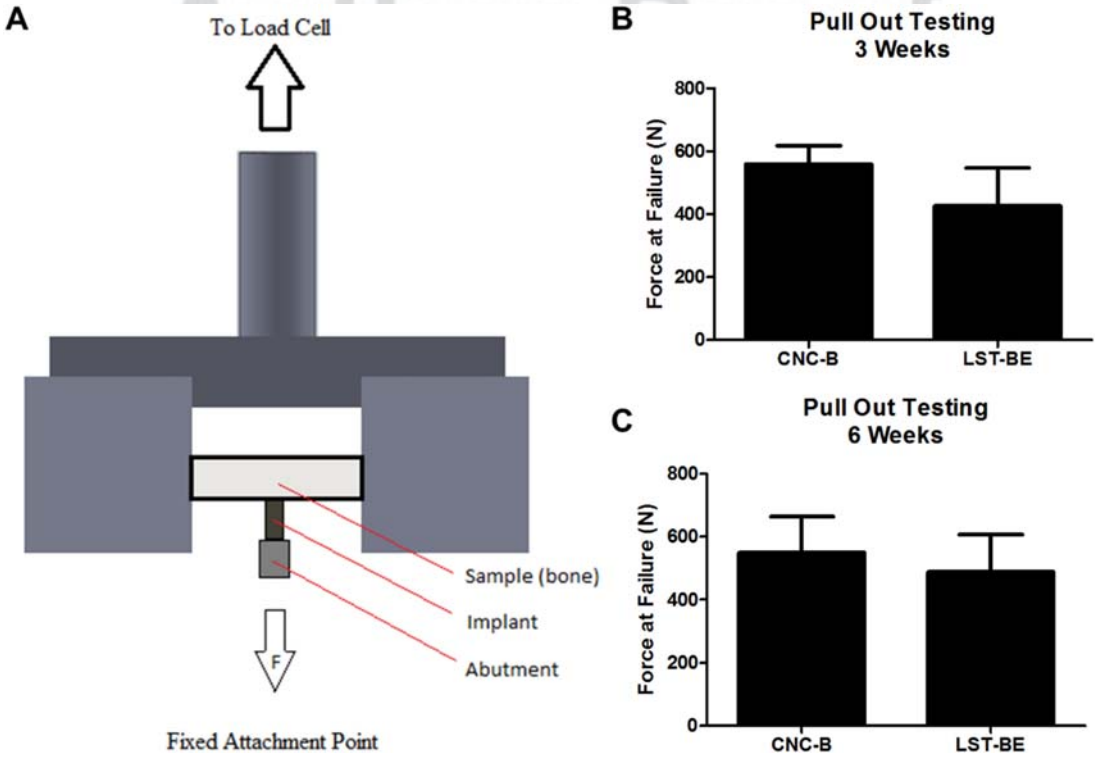

COLOR

FIGURE 7. A schematic of pull out mechanical testing of implants (A). Force at failure at 3 (B, $n = 3$ implants/type) and 6 weeks (C, $n = 5$ implants/type) after surgery in rabbits. Unpaired t test showed no difference between CNC-B and LST-BE implants.

MicroCT analysis

Osseointegration was achieved for both implant groups, and was compared using microCT analysis. BIC values obtained through microCT analysis were not significantly different between machined and LST-BE implants at 3 and 6 weeks F6 [Fig. 6(A)–(D)]. Additional analysis conducted on the superior cortical, trabecular, and inferior cortical regions of implants showed no difference in BIC values between CNC-B and LST-BE implants at 6 weeks [Fig. 6(E)].

Mechanical testing

The femur specimen was fixed in a custom-fabricated test device with the implant aligned to the machine axis to ensure that no bending moment was created during the test F7 [Fig. 7(A)]. Pullout mechanical testing revealed no significant differences between failure forces for CNC-B and LST-BE implants after 3 [Fig. 7(B)] and 6 [Fig. 7(C)] weeks. Values at 3 and 6 weeks for each implant type were comparable, with strong implant to bone stability.

DISCUSSION

Advanced manufacturing technologies such as laser sintering can produce Ti–6Al–4V constructs with potential use in the dental and orthopedic implant industries. In this study, laser sintering was used in conjunction with surface treatments to produce novel Ti–6Al–4V implant surfaces and implants with hierarchical micro- and nano-roughness and hydrophilicity that increased osteoblast response *in vitro* and osseointegration *in vivo*. Our results indicate that additive manufacturing is a viable method for producing dental implants leading to enhanced biological response, even when compared to a traditionally manufactured, currently used commercial implant.

Surface characterization of disks revealed a unique hierarchical micro-/nano-roughness of LST-BE surfaces with post-processing treatments. Although both blasting (LST-B) and blasting plus acid etching (LST-BE) resulted in this roughness, LCM analysis of roughness values showed higher S_a and S_z values for LST-BE surfaces than LST-B surfaces. Because surface micro-roughness was beyond the *z*-limit of currently existing atomic force microscopes, nano-roughness could be observed only qualitatively via SEM images.[34] In this study, all laser sintered surfaces were post-processed to remove any residual particles or debris remaining from the sintering process and to create a more homogeneous surface roughness that has been shown to result in better biological response.[10,12] The combination of micro- and nano-roughness on titanium and Ti–6Al–4V has been shown to increase osteoblast maturation, differentiation, and local factor production *in vitro*, and other studies have shown hierarchical roughness and hydrophilicity to be important for increasing osseointegration in animal models as well.[15,27,35–39]

LST-B surface contained much higher levels of oxygen than any other surface, indicating an increased oxide layer that was a result of the calcium phosphate blasting process. Studies have shown that oxygen retention can occur during the sintering process, even within an enclosed argon chamber.[40] Though grit blasting may have exposed these oxygen-rich sites, acid etching was able to alter the surface oxide. Traditionally, strong sulfuric and hydrochloric acids have been used to etch titanium surfaces to induce micro-roughness.[41] Additional aging over time in saline solution or a second oxidation processing step was required to overlay nanostructures on existing micro-roughness.[27,35,42] In this study, we were able to introduce both micro- and nano-roughness in just one etching step. Maleic and oxalic acids are commonly used to etch human enamel and dentin,[43] but this is the first report of the combination used to etch titanium. Although not characterized in this study, material mechanical properties can differ for cast and laser sintered Ti–6Al–4V.[11] As hardness and tensile strength can be directly affected by the thickness of the oxide layer, differences in mechanical properties may also be implicated in the biological response.[44]

In vitro studies suggest that LST-BE surfaces possess unique surface characteristics that increase osteoblast differentiation and maturation at the implant site, contribute to the differentiation of cells distal to the implant surface, contribute to the bone remodeling process by decreasing osteoclast resorption, and enhance blood vessel formation to further bone formation. Our lab has pioneered the MG63 cell line as a model for evaluating osteoblast response to surface topography and wettability, showing enhanced maturation for increasing surface roughness and hydrophilicity.[17,27,45,46] In this study, osteoblasts responded to surfaces in a maturation-dependent manner.

Osteocalcin, a late marker of osteoblast differentiation, has been shown to be regulated by both surface roughness and hydrophilicity in MG63 cells.[47] While immature osteoblast-like MG63 cells increased osteocalcin protein production on micro-/nano-rough, hydrophilic LST-B and LST-BE surfaces ~~than on~~ the smoother CNC-M and LST-M surfaces, the cells were not able to differentiate between the small changes in roughness between the surfaces examined. In contrast, mature NHOsts were more sensitive to small roughness changes in the absence of hydrophilicity, showing increased osteocalcin production on LST-M surfaces compared to slightly smoother CNC-M surfaces. However, NHOst osteocalcin production did not differ on the hydrophilic LST-B and LST-BE surfaces possessing a similar magnitude change in surface roughness.

Surface effects on OPG, a RANKL decoy receptor, for both cells were similar. Increased levels of OPG on rough surfaces suggest that surface roughness by itself can affect bone remodeling. By decreasing RANKL binding, secretion of OPG can inhibit osteoclast activity for increased net bone formation by osteoblasts. The increase in OPG on rough surfaces has been attributed to a similarity of surface micro-/nano-features with resorption pits in bone, indicating a possible explanation for the response to rough LST surfaces in our study.[48]

VEGF production by NHOsts showed a much more robust response to hierarchical surface roughness and hydrophilicity in comparison to VEGF production by MG63

J_ID: JBM Customer A_ID: JBMA35739 Cadmus Art: JBMA35739 Ed. Ref. No.: JBMR-A-15-0729.R1 Date: 11-April-16 Stage: Page: 11

cells. These results suggest that VEGF may play a more active role later in osteoblast maturation, contributing to continued blood vessel formation and bone integration. BMP2 expression in NHOst cells showed a differential response to small changes in roughness on hydrophilic surfaces LST-B and LST-BE while expression of MG63 cells was similar for both hydrophilic surfaces. Expression of these local factors is important for enhancing osteoblastic differentiation of mesenchymal stem cells distal to the implant, as our group has shown previously.[18] Taken together, our *in vitro* results align with previous observations ~~that~~ a more robust response to nanotopography by mature osteoblasts in comparison to undifferentiated mesenchymal stem cells, with this effect able to be modulated by surface wettability.[15,35]

Cell surface integrin receptors mediate cell response to biomaterials. In particular, integrin $\alpha2\beta1$ has been shown to play a significant role in the osteoblast and mesenchymal response to titanium surface roughness, though different integrin profiles may play a role depending on cell lineage.[18,49,50] In this study, we analyzed mRNA expression of $\alpha2$ and $\beta1$ integrin subunits, showing increased expression of both these subunits on rough LST-B and LST-BE surfaces compared to smooth CNC-M surfaces. The similar expression profiles of $\alpha2$ and $\beta1$ corroborate our theory that $\alpha2\beta1$ is responsible for osteoblast maturation and differentiation on micro-rough surfaces. The presence of hierarchical micro-/nano-roughness on our LST-B and LST-BE suggests that $\alpha2\beta1$ mediates cell response to surfaces at the nanoscale as well.

A variety of animal models have been used to study osseointegration of laser sintered implants.[21,51,52] We opted to use a rabbit model to compare osseointegration of LST-BE implants with osseointegration of CNC-B implants, which are used clinically. Although rabbits possess differences in bone structure and remodeling in comparison to humans, including a venous plexus within the tibial cortical bone, they have shown similar responses to implant roughness that are seen clinically, and are the most commonly used model for dental implant evaluation.[53–57] Due to faster skeletal change and bone turnover rates in rabbits compared to humans, studies have shown accelerated healing at 4 weeks.[58,59] To address the fact that most commonly implants are used in adult humans, we used ~~a~~ fully mature rabbit for the present study.

We evaluated BIC values at 3 and 6 weeks to understand the effects of implant manufacturing and differences in surface roughness on early events in osseointegration. Other studies evaluating osseointegration of implants placed in a similar femoral model in rabbits show new trabecular bone formation by 4 weeks, with continued bone remodeling and growth up to 42 weeks after implantation.[60,61] Though our study ended at 6 weeks, other studies have shown predictive osseointegration results in rabbits as early as 2 weeks after implantation.[55] It is possible that differences may have been observed at earlier time points. As with any small animal model where the implant cannot be placed directly in the jaw, mechanical loading will be different.[53] We believe that our model is valid for comparing osseointegration of endosseous implants and can be indicative of clinical outcomes. While BIC values showed improvement in osseointegration of LST-BE implants in comparison to CNC-B implants, further studies in disease challenged animal models or at longer time points may be necessary for elucidating the superiority of novel LST implants for improving osseointegration in compromised cases.

Although microCT evaluation of BIC has been compared to histomorphometric analysis with promising results, metal artifacts due to scattering continue to be a confounding factor in accurate microCT analysis.[62–64] We considered BIC values from both sources and found that histomorphometric analysis was more reliable in describing bone formation during the early stages of osseointegration. Although total BIC was not significantly different between CNC-B and LST-BE implants at 3 weeks, a higher amount of cortical bone was seen in LST-BE implants compared to CNC-B implants. The change in the composition of trabecular and cortical bone between 3 and 6 weeks was evident as well, which was observed at the same time points in a similar implantation model.[65] Total BIC values were higher for LST-BE implants compared to CNC-B implants at 6 weeks, with a significantly reduced trabecular LST BIC compared to total BIC. This reduction was not seen in either implant group at 3 weeks, suggesting increased bone remodeling of LST-BE implants during the osseointegration process as compared to that of CNC-B implants.

Differences in BIC values can also be attributed to the analysis in different planes. BIC analysis was performed on sagittal cross sections throughout the entire implant for microCT, whereas analysis was carried out on transaxial cross sections for histology. Mechanical testing was performed to verify osseointegration of implants further. Similar pullout forces for both implants indicate that LST-BE implants achieved good mechanical stability, which was comparable to that of the commercially used CNC-B implant. These results suggest that LST-BE implants are similar to, if not better than traditional CNC-B manufactured implants. The enhanced biological response can be attributed to the LST-BE's unique surface properties and ability to promote osteoblast maturation and differentiation at and distal to the surface, influence bone remodeling and increase blood vessel formation for increased osseointegration.

CONCLUSION

Laser sintering is an additive manufacturing technique that can produce Ti–6Al–4V implants. The implants can be further processed to create micro-rough, nano-rough, and hydrophilic surfaces. The resulting surface with combined roughness and wettability enhanced both MG63 and NHOst cell response in comparison to smooth CNC-M and LST-M surfaces. LST-BE implants were compared to commercially available CNC-B implants in a healthy animal model, and cortical BIC was higher at 3 weeks and total BIC higher at 6 weeks than CNC implants. LST-BE and CNC-B implants had similar pullout forces at both time points examined,

ID: pachiyappanm Time: 20:01 I Path: //chenas03/Cenpro/ApplicationFiles/Journals/Wiley/JBMM/Vol00000/160095/Comp/APPFile/JW-JBMM160095

indicating that LST-BE implants are as mechanically stabile as clinically used implants. These results suggest that implants produced by laser sintering with combined micro-/nano-roughness and high surface energy are a suitable alternative to traditionally manufactured endosseous implants, with favorable biological response and ability to osseointegrate.

ACKNOWLEDGMENTS

The authors would like to thank AB Dental for the surfaces and implants used this study. The content is solely the responsibility of the authors; it does not necessarily represent the official views of the National Institutes of Health.

REFERENCES

1. Van Noort R. Titanium: The implant material of today. J Mater Sci 1987;22:3801–3811.
2. McCracken M. Dental implant materials: Commercially pure titanium and titanium alloys. J Prosthodont 1999;8:40–43.
3. Elias CN, Lima JHC, Valiev R, Meyers MA. Biomedical applications of titanium and its alloys. Jom 2008;60:46–49.
4. Pjetursson BE, Asgeirsson AG, Zwahlen M, Sailer I. Improvements in implant dentistry over the last decade: Comparison of survival and complication rates in older and newer publications. Int J Oral Maxillofac Implants 2014;29:308–324.
5. Corbett KL, Losina E, Nti AA, Prokopetz JJZ, Katz JN. Population-based rates of revision of primary total hip arthroplasty: A systematic review. PLoS One 2010;5:e13520
6. Mellado-Valero A, Ferrer Garcia JC, Herrera Ballester A, Labaig Rueda C. Effects of diabetes on the osseointegration of dental implants. Med Oral Patol Oral Cir Bucal 2007;12:E38–E43.
7. Aro HT, Alm JJ, Moritz N, Makinen TJ, Lankinen P. Low bmd affects initial stability and delays stem osseointegration in cementless total hip arthroplasty in women: A 2-year RSA study of 39 patients. Acta Orthop 2012;83:107–114.
8. Kasat V, Ladda R. Smoking and dental implants. J Int Soc Prev Community Dent 2012;2:38–41.
9. McGuire MK, Wilson TG Jr. Commentary: From normal scientific progress to game changers: The impact on periodontal clinical practice. J Periodontol 2014;85:1001–1005.
10. Traini T, Mangano C, Sammons RL, Mangano F, Macchi A, Piattelli A. Direct laser metal sintering as a new approach to fabrication of an isoelastic functionally graded material for manufacture of porous titanium dental implants. Dent Mater 2008;24:1525–1533.
11. Murr LE, Quinones SA, Gaytan SM, Lopez MI, Rodela A, Martinez EY, Hernandez DH, Martinez E, Medina F, Wicker RB. Microstructure and mechanical behavior of Ti–6Al–4V produced by rapid-layer manufacturing, for biomedical applications. J Mech Behav Biomed Mater 2009;2:20–32.
12. Cheng A, Humayun A, Cohen DJ, Boyan BD, Schwartz Z. Additively manufactured 3D porous Ti–6Al–4V constructs mimic trabecular bone structure and regulate osteoblast proliferation, differentiation and local factor production in a porosity and surface roughness dependent manner. Biofabrication 2014;6:045007
13. Amin Yavari S, van der Stok J, Chai YC, Wauthle R, Tahmasebi Birgani Z, Habibovic P, Mulier M, Schrooten J, Weinans H, Zadpoor AA. Bone regeneration performance of surface-treated porous titanium. Biomaterials 2014;35:6172–6181.
14. Cohen DJ, Cheng A, Kahn A, Aviram M, Whitehead AJ, Hyzy SL, Clohessy RM, Boyan BD, Schwartz Z. Novel osteogenic Ti–6Al–4V device for restoration of dental function in patients with large bone deficiencies: Design, development and implementation. Sci Rep 2016;6:20493
15. Gittens RA, Olivares-Navarrete R, Cheng A, Anderson DM, McLachlan T, Stephan I, Geis-Gerstorfer J, Sandhage KH, Fedorov AG, Rupp F, et al. The roles of titanium surface micro/nanotopography and wettability on the differential response of human osteoblast lineage cells. Acta Biomater 2013;9:6268–6277.
16. Schwarz F, Ferrari D, Herten M, Mihatovic I, Wieland M, Sager M, Becker J. Effects of surface hydrophilicity and microtopography on early stages of soft and hard tissue integration at non-submerged titanium implants: An immunohistochemical study in dogs. J Periodontol 2007;78:2171–2184.
17. Zhao G, Schwartz Z, Wieland M, Rupp F, Geis-Gerstorfer J, Cochran DL, Boyan BD. High surface energy enhances cell response to titanium substrate microstructure. J Biomed Mater Res A 2005;74A:49–58.
18. Olivares-Navarrete R, Hyzy SL, Hutton DL, Erdman CP, Wieland M, Boyan BD, Schwartz Z. Direct and indirect effects of microstructured titanium substrates on the induction of mesenchymal stem cell differentiation towards the osteoblast lineage. Biomaterials 2010;31:2728–2735.
19. Kopf BS, Ruch S, Berner S, Spencer ND, Maniura-Weber K. The role of nanostructures and hydrophilicity in osseointegration: In-vitro protein-adsorption and blood-interaction studies. J Biomed Mater Res A 2015,
20. Olivares-Navarrete R, Raines AL, Hyzy SL, Park JH, Hutton DL, Cochran DL, Boyan BD, Schwartz Z. Osteoblast maturation and new bone formation in response to titanium implant surface features are reduced with age. J Bone Miner Res 2012;27,
21. de Wild M, Schumacher R, Mayer K, Schkommodau E, Thoma D, Bredell M, Kruse Gujer A, Gratz KW, Weber FE. Bone regeneration by the osteoconductivity of porous titanium implants manufactured by selective laser melting: A histological and micro computed tomography study in the rabbit. Tissue Eng Part A 2013;19:2645–2654.
22. Veltri M, Ferrari M, Balleri P. Correlation of radiographic fractal analysis with implant insertion torque in a rabbit trabecular bone model. Int J Oral Maxillofac Implants 2011;26:108–114.
23. He FM, Yang GL, Zhao SF, Cheng ZP. Mechanical and histomorphometric evaluations of rough titanium implants treated with hydrofluoric acid/nitric acid solution in rabbit tibia. Int J Oral Maxillofac Implants 2011;26:115–122.
24. Thorey F, Menzel H, Lorenz C, Gross G, Hoffmann A, Windhagen H. Osseointegration by bone morphogenetic protein-2 and transforming growth factor beta2 coated titanium implants in femora of New Zealand white rabbits. Indian J Orthop 2011;45:57–62.
25. Neyt JG, Buckwalter JA, Carroll NC. Use of animal models in musculoskeletal research. Iowa Orthop J 1998;18:118–123.
26. Rupp F, Gittens RA, Scheideler L, Marmur A, Boyan BD, Schwartz Z, Geis-Gerstorfer J. A review on the wettability of dental implant surfaces I: Theoretical and experimental aspects. Acta Biomater 2014;10:2894–2906.
27. Gittens RA, McLachlan T, Olivares-Navarrete R, Cai Y, Berner S, Tannenbaum R, Schwartz Z, Sandhage KH, Boyan BD. The effects of combined micron-/submicron-scale surface roughness and nanoscale features on cell proliferation and differentiation. Biomaterials 2011;32:3395–3403.
28. Olivares-Navarrete R, Gittens RA, Schneider JM, Hyzy SL, Haithcock DA, Ullrich PF, Schwartz Z, Boyan BD. Osteoblasts exhibit a more differentiated phenotype and increased bone morphogenetic protein production on titanium alloy substrates than on poly-ether-ether-ketone. Spine J 2012;12:265–272.
29. del Cerro M, Cogen J, del Cerro C. Stevenel's blue, an excellent stain for optical microscopical study of plastic embedded tissues. Microsc Acta 1980;83:117–121.
30. Maniatopoulos C, Rodriguez A, Deporter DA, Melcher AH. An improved method for preparing histological sections of metallic implants. Int J Oral Maxillofac Implants 1986;1:31–37.
31. Lillie RD, Conn HJ. Biological Stains: A Handbook on the Nature and Uses of the Dyes Employed in the Biological Laboratory. Baltimore: Williams and Wilkins; 1977.
32. Salou L, Hoornaert A, Louarn G, Layrolle P. Enhanced osseointegration of titanium implants with nanostructured surfaces: An experimental study in rabbits. Acta Biomater 2015;11:494–502.
33. Brånemark R, Öhrnell L-O, Nilsson P, Thomsen P. Biomechanical characterization of osseointegration during healing: An experimental in vivo study in the rat. Biomaterials 1997;18:969–978.
34. Hotchkiss KM, Reddy GB, Hyzy SL, Schwartz Z, Boyan BD, Olivares-Navarrete R. Titanium surface characteristics, including

topography and wettability, alter macrophage activation. Acta Biomater 2016;31:425–434.
35. Gittens RA, Olivares-Navarrete R, McLachlan T, Cai Y, Hyzy SL, Schneider JM, Schwartz Z, Sandhage KH, Boyan BD. Differential responses of osteoblast lineage cells to nanotopographically-modified, microroughened titanium–aluminum–vanadium alloy surfaces. Biomaterials 2012;33:8986–8994.
36. Gittens RA, Olivares-Navarrete R, Schwartz Z, Boyan BD. Implant osseointegration and the role of microroughness and nanostructures: Lessons for spine implants. Acta Biomater 2014;10:3363–3371.
37. Wennerberg A, Jimbo R, Stübinger S, Obrecht M, Dard M, Berner S. Nanostructures and hydrophilicity influence osseointegration: A biomechanical study in the rabbit tibia. Clin Oral Implants Res 2014;25:1041–1050.
38. Olivares-Navarrete R, Hyzy SL, Gittens RAs, Schneider JM, Haithcock DA, Ullrich PF, Slosar PJ, Schwartz Z, Boyan BD. Rough titanium alloys regulate osteoblast production of angiogenic factors. Spine J 2013;13:1563–1570.
39. Olivares-Navarrete R, Hyzy SL, Slosar PJ, Schneider JM, Schwartz Z, Boyan BD. Implant materials generate different peri-implant inflammatory factors: Poly-ether-ether-ketone promotes fibrosis and microtextured titanium promotes osteogenic factors. Spine 2015;40:399–404.
40. Santos EC, Osakada K, Shiomi M, Kitamura Y, Abe F. Microstructure and mechanical properties of pure titanium models fabricated by selective laser melting. Proc Inst Mech Eng C J Mech Eng Sci 2004;218:711–719.
41. Li D, Ferguson SJ, Beutler T, Cochran DL, Sittig C, Hirt HP, Buser D. Biomechanical comparison of the sandblasted and acid-etched and the machined and acid-etched titanium surface for dental implants. J Biomed Mater Res 2002;60:325–332.
42. Wennerberg A, Svanborg LM, Berner S, Andersson M. Spontaneously formed nanostructures on titanium surfaces. Clin Oral Implants Res 2013;24:203–209.
43. Fanchi M, Breschi L. Effects of acid-etching solutions on human enamel and dentin. Quintessence Int 1995;26:431–435.
44. Oh JM, Lee BG, Cho SW, Lee SW, Choi GS, Lim JW. Oxygen effects on the mechanical properties and lattice strain of Ti and Ti–6Al–4V. Met Mater Int 2011;17:733–736.
45. Martin JY, Schwartz Z, Hummert TW, Schraub DM, Simpson J, Lankford J, Dean DD, Cochran DL, Boyan BD. Effect of titanium surface roughness on proliferation, differentiation, and protein synthesis of human osteoblast-like cells (MG63). J Biomed Mater Res 1995;29:389–401.
46. Lincks J, Boyan BD, Blanchard CR, Lohmann CH, Liu Y, Cochran DL, Dean DD, Schwartz Z. Response of MG63 osteoblast-like cells to titanium and titanium alloy is dependent on surface roughness and composition. Biomaterials 1998;19:2219–2232.
47. Gittens RA, Scheideler L, Rupp F, Hyzy SL, Geis-Gerstorfer J, Schwartz Z, Boyan BD. A review on the wettability of dental implant surfaces II: Biological and clinical aspects. Acta Biomater 2014;10:2907–2918.
48. Zinger O, Zhao G, Schwartz Z, Simpson J, Wieland M, Landolt D, Boyan B. Differential regulation of osteoblasts by substrate microstructural features. Biomaterials 2005;26:1837–1847.
49. Olivares-Navarrete R, Raz P, Zhao G, Chen J, Wieland M, Cochran DL, Chaudhri RA, Ornoy A, Boyan BD, Schwartz Z. Integrin $\alpha 2\beta 1$ plays a critical role in osteoblast response to micron-scale surface structure and surface energy of titanium substrates. Proc Natl Acad Sci U S A 2008;105:15767–15772.
50. Olivares-Navarrete R, Hyzy SL, Berg ME, Schneider JM, Hotchkiss K, Schwartz Z, Boyan BD. Osteoblast lineage cells can discriminate microscale topographic features on titanium–aluminum–vanadium surfaces. Ann Biomed Eng 2014;42:2551–2561.
51. Pattanayak DK, Fukuda A, Matsushita T, Takemoto M, Fujibayashi S, Sasaki K, Nishida N, Nakamura T, Kokubo T. Bioactive Ti metal analogous to human cancellous bone: Fabrication by selective laser melting and chemical treatments. Acta Biomater 2011;7:1398–1406.
52. Mangano F, Chambrone L, van Noort R, Miller C, Hatton P, Mangano C. Direct metal laser sintering titanium dental implants: A review of the current literature. Int J Biomater 2014;2014:461534
53. Mapara M, Thomas BS, Bhat KM. Rabbit as an animal model for experimental research. Dent Res J 2012;9:111–118.
54. Yang GL, He FM, Yang XF, Wang XX, Zhao SF. Bone responses to titanium implants surface-roughened by sandblasted and double etched treatments in a rabbit model. Oral Surg Oral Med Oral Pathol Oral Radiol Endod 2008;106:516–524.
55. Le Guehennec L, Goyenvalle E, Lopez-Heredia M-A, Weiss P, Amouriq Y, Layrolle P. Histomorphometric analysis of the osseointegration of four different implant surfaces in the femoral epiphyses of rabbits. Clin Oral Implants Res 2008;19:1103–1110.
56. Götz HE, Müller M, Emmel A, Holzwarth U, Erben RG, Stangl R. Effect of surface finish on the osseointegration of laser-treated titanium alloy implants. Biomaterials 2004;25:4057–4064.
57. Coelho PG, Granjeiro JM, Romanos GE, Suzuki M, Silva NRF, Cardaropoli G, Thompson VP, Lemons JE. Basic research methods and current trends of dental implant surfaces. J Biomed Mater Res B Appl Biomater 2009;88B:579–596.
58. Sollazzo V, Pezzetti F, Scarano A, Piattelli A, Bignozzi CA, Massari L, Brunelli G, Carinci F. Zirconium oxide coating improves implant osseointegration in vivo. Dent Mater 2008;24:357–361.
59. Pearce AI, Richards RG, Milz S, Schneider E, Pearce SG. Animal models for implant biomaterial research in bone: A review. Eur Cell Mater 2007;13:1–10.
60. Suzuki K, Aoki K, Ohya K. Effects of surface roughness of titanium implants on bone remodeling activity of femur in rabbits. Bone 1997;21:507–514.
61. Sennerby L, Thomsen P, Ericson LE. Early tissue response to titanium implants inserted in rabbit cortical bone. J Mater Sci Mater Med 1993;4:240–250.
62. Liu S, Broucek J, Virdi AS, Sumner DR. Limitations of using micro computed tomography to predict bone-implant contact and mechanical fixation. J Microsc 2012;245:34–42.
63. Butz F, Ogawa T, Chang T-L, Nishimura I. Three-dimensional bone-implant integration profiling using micro-computed tomography. Int J Oral Maxillofac Implants 2006;21:687–695.
64. Vandeweghe S, Coelho PG, Vanhove C, Wennerberg A, Jimbo R. Utilizing micro-computed tomography to evaluate bone structure surrounding dental implants: A comparison with histomorphometry. J Biomed Mater Res B Appl Biomater 2013;101:1259–1266.
65. Pak H-S, Yeo I-S, Yang J-H. A histomorphometric study of dental implants with different surface characteristics. J Adv Prosthodont 2010;2:142–147.

AQ1: Please check whether the grant info is OK.
AB Dental should be separated from NSF.
AQ2: To Editor: Please check whether the placement is OK.
The placement is acceptable.
AQ3: Please provide the names of all the authors instead of others in Reference 15.
This reference has been updated (see comment).
AQ4: Please provide volume and page range for Ref. 19.
This reference has been updated (see comment).
AQ5: Please provide page range for Ref. 20.
This reference has been updated (see comment).
AQ6: Please confirm that given names (red) and surnames/family names (green) have been identified correctly.
The names have been identified correctly.

Please confirm that the funding sponsor list below was correctly extracted from your article: that it includes all funders and that the text has been matched to the correct FundRef Registry organization names. If a name was not found in the FundRef registry, it may be not the canonical name form or it may be a program name rather than an organization name or it may be an organization not yet included in FundRef Registry. If you know of another name form or a parent organization name for a not found item on this list below, please share that information.

FundRef name	FundRef Organization Name (Country)	FundRef DOI	Grant IDs
AB Dental and National Science Foundation Graduate Research Fellowship (to A.C.)	[NOT FOUND IN FUNDREF REGISTRY]		
SNI program from SENACYT, Panama (R.A.G.)	Alaska Space Grant Program Association of Schools and Programs of Public Health Australian Coal Association Research Program California Department of Alcohol and Drug Programs Canadian Child Health Clinician Scientist Program [NOT FOUND IN FUNDREF REGISTRY]		
National Institute of Arthritis and Musculoskeletal and Skin Diseases (NIAMS) (USPHS Award Nos. AR052102 and AR068703)	National Institute of Arthritis and Musculoskeletal and Skin Diseases	10.13039/100000069	